

# On the Viability of Semi-Supervised Segmentation Methods for Statistical Shape Modeling

Asma Khan<sup>1,2,\*</sup>

ASMAK@SCI.UTAH.EDU

Tushar Kataria<sup>1,2,\*</sup>

TUSHAR.KATARIA@SCI.UTAH.EDU

Janmesh Ukey<sup>1,2</sup>

JANMESH@SCI.UTAH.EDU

Shireen Elhabian<sup>1,2</sup>

SHIREEN@SCI.UTAH.EDU

<sup>1</sup> Kahlert School of Computing, University of Utah, Salt Lake City, USA,

<sup>2</sup> Scientific Computing and Imaging Institute, University of Utah, Salt Lake City, USA

\* Equal Contribution

**Editors:** Under Review for MIDL 2025

## Abstract

Statistical Shape Models (SSMs) excel at identifying population level anatomical variations, which is at the core of various clinical and biomedical applications, including morphology-based diagnostics and surgical planning. However, the effectiveness of SSM is often constrained by the necessity for expert-driven manual segmentation, a process that is both time-intensive and expensive, thereby restricting their broader application and utility. Recent deep learning approaches enable the direct estimation of Statistical Shape Models (SSMs) from unsegmented images. While these models can predict SSMs without segmentation during deployment, they do not address the challenge of acquiring the manual annotations needed for training, particularly in resource-limited settings. Semi-supervised models for anatomy segmentation can mitigate the annotation burden. Yet, despite the abundance of available approaches, there are no established guidelines to inform end-users on their effectiveness for the downstream task of constructing SSMs. In this study, we systematically evaluate the potential of semi-supervised methods as viable alternatives to manual segmentations for building SSMs. We establish a new performance benchmark by employing various semi-supervised methods for anatomy segmentation under low annotation settings, utilizing the predicted segmentation’s for the task of SSM. Our results indicate that some methods produce noisy segmentation, which is very unfavorable for SSM tasks, while others can capture the correct modes of variations in the population cohort with 60-80% reduction in required manual annotation.

**Keywords:** Statistical Shape Modeling, Semi Supervised Segmentation Study

## 1. Introduction

Statistical shape models (SSMs) provide a quantitative means for analyzing anatomical variations across populations, enabling the identification of normative trends and deviations and facilitating the development of diagnostic tools and surgical planning systems (Goparaju et al., 2022). Constructing SSMs is contingent upon the accurate segmentation of the target anatomy. This process is both time-consuming and resource-intensive, often hindered by the scarcity of medical expertise necessary for precise segmentation. Recent advances in deep learning have facilitated the direct estimation of SSMs from unsegmented images, thus bypassing the need for segmentation during inference (Bhalodia et al., 2018; Adams et al., 2020; Adams and Elhabian, 2022; Tao et al., 2022; Milletari et al., 2017; Xie et al.,

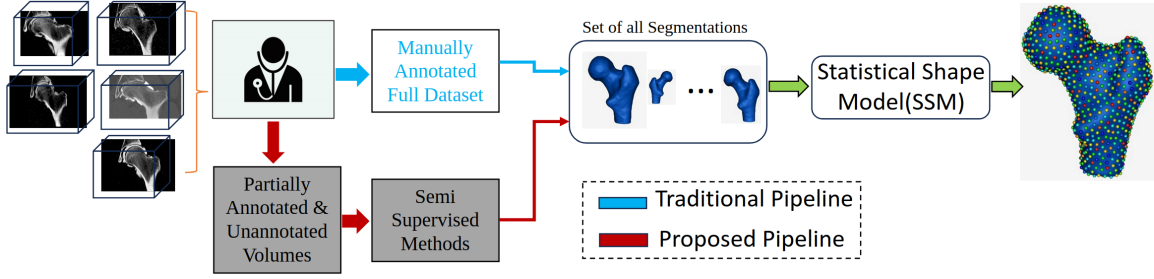


Figure 1: **Can manual annotation in constructing shape models be replaced by semi-supervised segmentation methods?** Figure shows the proposed new pipeline using Semi-supervised methods.

2016; Raju et al., 2022; Karanam et al., 2023; Bhalodia et al., 2024; Ukey and Elhabian, 2023; Ukey et al., 2024; Bhalodia et al., 2024; Xu and Elhabian, 2023; Iyer and Elhabian, 2023; Iyer et al., 2024; Adams et al., 2024). However, these deep learning methods still necessitate anatomy segmentation to construct SSMs for training.

Automated or deep learning based anatomy segmentation can mitigate the segmentation burden for constructing SSMs; however, networks designed for segmentation task still require significant manual annotations for their training. To alleviate such burden, a variety of semi-supervised approaches have been developed, each demonstrating different levels of performance. Semi-supervised methods (e.g., (Goparaju et al., 2022; Luo et al., 2021; Bai et al., 2023; Yu et al., 2019; Tarvainen and Valpola, 2017)), typically leverage a subset of fully annotated volumes alongside all unannotated volumes for model training. These methods use a combination of clever data augmentations (Bai et al., 2023), pseudo labelling (Bai et al., 2023; Tarvainen and Valpola, 2017; Yu et al., 2019), consistency regularization (Tarvainen and Valpola, 2017; Wu et al., 2021), and entropy minimization (Vu et al., 2019) to obtain high quality segmentation’s. A few of these methods (e.g., (Li et al., 2022; Yeung et al., 2021; Nihalaani et al., 2024)) exploit the inherent 3D structure of the input image, allowing for the reduction of annotation requirements from entire volumes to individual slices. Currently, numerous annotation-efficient methods exist for anatomy segmentation. However, there are no established guidelines to evaluate their suitability as alternatives to manual segmentation for constructing SSMs.

In this paper, we present a comprehensive benchmark for evaluating the performance of Shape Statistical Models constructed using prediction generated by semi-supervised segmentation techniques. By leveraging these weak supervision methods, we aim to reduce the reliance on fully annotated data in building SSMs, thereby enhancing the accessibility and practical use of SSM tools. Our analysis aims to determine which weakly supervised approaches are suitable for downstream population level statistical analysis (SSMs). To this end, our benchmark compares SSMs obtained from various semi-supervised segmentation methods against SSMs derived from manual annotations (ground truth, or upper bound in performance), assessing their effectiveness in settings with limited labeled data (as shown in Figure 1). The main contributions of this manuscript are:

- We benchmark semi-supervised SSM by comparing SSMs trained on manual segmentations with those derived from semi-supervised methods across two datasets.

- A comprehensive quantitative and qualitative analysis for downstream SSM applications, highlighting the failure modes of current semi-supervised methods.

## 2. Methods

To determine whether semi-supervised methods can effectively replace manual annotations for SSM, we seek to address the following key questions:-

- *Do SSM models created using semi-supervised model predictions capture the same modes of variation compared to an SSM model using all manual segmentations ?*
- *Are some semi-supervised methods more reliable than others ?*
- *Does increasing the amount of annotated data for semi-supervised models improve SSM for the population cohort?*

### 2.1. Selected Semi-Supervised Methods.

Semi-supervised medical image segmentation leverages partially labeled and all unlabeled data during training. We selected eight distinct methods that utilize labeled and unlabeled data in various ways, categorizing them into three distinct groups: (A) *Student-teacher methods*:- Mean Teacher (MT)(Tarvainen and Valpola, 2017) & Uncertainty Mean Teacher (UA-MT)(Yu et al., 2019), (B) *Pseudo-labeling methods*:- Mutual Correction Framework (MCF) (Wang et al., 2023b), Orthogonal Annotation (DeSCO) (Cai et al., 2023), Bidirectional Copy-Paste (BCP)(Bai et al., 2023) and Correlation-Aware Mutual Learning (CAML) (Gao et al., 2023), and (C) *Multi-task learning methods*:- Dual-task Consistency (DTC) (Cai et al., 2023), and Shape-Aware Semi-supervised (SASSnet) (Li et al., 2020). A brief description of each of these methods is added below:

**Mean Teacher (MT)(Tarvainen and Valpola, 2017).** Mean Teacher uses consistency regularization between *student-teacher* training paradigm. The *student* model is trained using the supervised loss on the labelled set, where as the *teacher*'s parameters are updated as an exponential moving average of the student model. Consistency loss on unlabelled data aligns the prediction between the two models.

**Uncertainty Mean Teacher (MT-UC)(Yu et al., 2019).** An extension of MT where the *teacher* model also estimates the uncertainty of each target prediction with Monte Carlo sampling. The uncertainty is used to preserve only the reliable predictions when calculating the consistency loss.

**Mutual Correction Framework (MCF) (Wang et al., 2023b).** MCF employs a student-teacher model paradigm to address cognitive biases learned during training, applying a rectification loss in regions where the model frequently makes errors. It then uses the Dice scores of segmentations predicted by both models to determine the pseudo-labels for unlabeled data.

**Bidirectional Copy-Paste (BCP)(Bai et al., 2023).** BCP integrates a bidirectional copy-paste framework into the Mean Teacher architecture. The student network receives inputs created by pasting random crops from labeled images onto unlabeled images and vice versa (bi-direction copy). The supervision of the *student* network involves combining both ground-truth labels and pseudo-labels generated by the *teacher* network using the same bidirectional copy-paste process.

**Correlation-Aware Mutual Learning (CAML)** (Gao et al., 2023). CAML introduces two modules: Cross-sample Mutual Attention, which uses transformers to compute attention between labeled and unlabeled samples within the same batch, and Omni-Correlation Consistency, a contrastive loss based on pixel-level latent space projections between labeled and unlabeled volumes. These modules enhance the transfer of information between labeled and unlabeled data, leading to improved segmentation performance.

**Orthogonal Annotation (DeSCO)** (Cai et al., 2023). This paper presents a novel orthogonal annotation strategy for semi-supervised 3D medical image segmentation, where only two orthogonal slices are labeled and the remaining volumes are unlabeled. It employs cross-consistency and pseudo-labeling to enhance performance. This method significantly reduces the annotation effort required, making it more feasible for broader deployment.

**Dual-task Consistency (DTC)** (Cai et al., 2023). Instead of applying consistency loss between labeled and unlabeled data, as seen in MT (Tarvainen and Valpola, 2017), UA-MT (Yu et al., 2019), and similar methods (Wu et al., 2021), DTC introduces a multi-task network to enforce consistency between two tasks. The chosen tasks are segmentation and level-set prediction, where the level-set function’s zero level corresponds to the contour of the segmented anatomy. The model is trained to ensure consistent predictions across both tasks for both labeled and unlabeled data.

**Shape-Aware Semi-supervised (SASSnet)** (Li et al., 2020). SASSnet introduces a shape-aware semi-supervised strategy that leverages multitasking to predict both segmentation and the signed distance map (SDM) simultaneously. Additionally, it employs an adversarial loss between the SDM predictions for labeled and unlabeled data, encouraging the model to learn shape-aware features more effectively.

## 2.2. Experimental Design

To offer a thorough evaluation of semi-supervised methods for constructing Statistical Shape Models (SSM), we design two experimental strategies that enable detailed analysis and support the future deployment of these methods for end-user applications.

Consider a dataset  $\mathcal{D}$ , which consists of a collection of anatomical images ( $\mathcal{I}$ ) along with their corresponding manual segmentations ( $\mathcal{S}$ ). The dataset is split into training  $\mathcal{D}_{Train}$  and testing set  $\mathcal{D}_{Test}$ , such that  $\mathcal{D}_{Train} \cap \mathcal{D}_{Test} = \emptyset$  and  $\mathcal{D}_{Train} \cup \mathcal{D}_{Test} = \mathcal{D}$ . We define the SSM representation of an anatomy as  $\Phi$ . The SSM is formulated as an optimization process aimed at minimizing the entropy of particles (or point clouds) on the surface of the anatomy (Cates et al., 2017). This process is applied to all segmentations in the training dataset, denoted as  $\mathcal{F}_{\Phi}(\cdot)$ , where the function parameters consist of the segmentations and the initial particle locations.  $\Phi_{Train}$  establishes the best training SSM representation, as it utilizes all the manual annotations in the training set to construct an SSM, as described by the equation below:

$$\Phi_{Train} = \arg \min_{\Phi} \mathcal{F}_{\Phi}(\mathcal{S}_i, \phi_0) \quad \forall i \in \mathcal{D}_{Train} \quad (1)$$

where  $\phi_0$  represents the initial condition.  $\phi_0$  it is set to origin for all particles. To generate the test SSM, we apply the same optimization over the test segmentations, with the  $\Phi_{Train}$  as initial condition (fixed domain initialization (Bhalodia et al., 2024)),

$$\Phi_{Test} = \arg \min_{\Phi} \mathcal{F}_{\Phi}(\mathcal{S}_i, \Phi_{Train}) \quad \forall i \in \mathcal{D}_{Test} \quad (2)$$



$\Phi_{Test}$  represents the upper bound SSM on the test set, reflecting the optimal SSM representation achievable using all manual annotations. However, since these test samples are unseen by the SSM model, distribution shifts between the training and test segmentations—such as variations in size and contour—can result in generalization errors.

Let us denote all selected semi-supervised methods discussed above as a set called  $SEMI \in \{MT, UA-MT, BCP, CAML, DeSCO, DTC, MCF, SASSnet\}$ . The predicted segmentations from these methods can be represented by  $\tilde{S}^k \forall k \in SEMI$ . To evaluate the potential of semi-supervised methods as an alternative to manual segmentations in SSM construction, we investigate two modeling strategies:

- **$\Phi_{Train}$  available (strategy 1):** Instead of using manual segmentations as in equation 2, predicted segmentations from each semi-supervised method ( $k \in SEMI$ ) on the test set are used to obtain the SSM representation as,

$$\tilde{\Phi}_{Test}^k = \arg \min_{\Phi} \mathcal{F}_{\Phi}(\tilde{S}_i^k, \Phi_{Train}) \quad \forall i \in \mathcal{D}_{Test} \quad (3)$$

compared to  $\Phi_{Test}$ ,  $\tilde{\Phi}_{Test}^k$  includes errors from both distribution shifts between the training and test segmentations and the absence of manual annotations for test set.

- **$\Phi_{Train}$  not available (strategy 2):** This strategy further limits access to manual segmentations by assuming that none are available for SSM representation on the training set. Only a small amount of segmentation data (20% or 40% of manual segmentations) are provided to train the semi-supervised methods, which then generate predicted segmentations for both the training and test sets. For each semi-supervised method ( $k \in SEMI$ ) we obtain the SSM representation of the training set as:

$$\tilde{\Phi}_{Train}^k = \arg \min_{\Phi} \mathcal{F}_{\Phi}(\tilde{S}_i^k, \phi_0) \quad \forall i \in \mathcal{D}_{Train} \quad (4)$$

where  $\phi_0$  is the initial condition. Using  $\tilde{\Phi}_{Train}^k$  representation, we create test SSM as,

$$\tilde{\Phi}_{Test}^k = \arg \min_{\Phi} \mathcal{F}_{\Phi}(\tilde{S}_i^k, \tilde{\Phi}_{Train}^k) \quad \forall i \in \mathcal{D}_{Test} \quad (5)$$

compared to  $\Phi_{Test}$ , the  $\tilde{\Phi}_{Test}^k$  representation is impacted by the same errors from strategy 1, with the added impact due to absence of manual segmentations on the training set.

### 2.3. Datasets and Metrics for Performance Evaluation

**Datasets Used.** We used two datasets: one public and one in-house. For the public dataset, we used the NAMIC Left Atrium segmentation dataset from (Bhalodia et al., 2024). Our in-house dataset (FEMUR) comprised 49 volumes, with 40 allocated for training and the remaining 9 for testing. Additional Dataset and implementation detail in Appendix A.

**Segmentation Metrics.** We use Dice scores to report the accuracy of the semi-supervised segmentation model (Tarvainen and Valpola, 2017; Yu et al., 2019; Kataria et al., 2023; Wang et al., 2023b; Kataria et al., 2024), additional metrics such as Jaccard score, Average surface distance and Hausdorff distance are reported in Appendix.

**SSM metrics.** All the training and testing SSMs created above are compared qualitatively by comparing their first and second mode of variations. For quantitative analysis four metrics: compactness (Cates et al., 2017; Adams et al., 2024; Bhalodia et al., 2024), specificity (Cates et al., 2017; Adams et al., 2024; Bhalodia et al., 2024), generalization (Cates et al., 2017; Adams et al., 2024; Bhalodia et al., 2024) and grassmannian distance. All these metrics are defined on PCA projection obtained from train/test SSMs particle. **Compactness:** A more compact SSM requires fewer PCA modes/parameters, so a higher area under the curve(AUC) indicates better compactness. **Specificity:** Measures if the predicted SSM produces valid shape instances, calculated as the average distance between training examples and generated samples from PCA embeddings using different components, therefore lower is better. Compactness and Specificity are only reported for training SSMs (Cates et al., 2017; Adams et al., 2024; Bhalodia et al., 2024), as training SSM in strategy 1 is always on ground truth data, we do not report these metrics for strategy 1. **Generalization:** A generalizable SSM transfers well to unseen subjects. This metric evaluates the distance between test particle correspondences and their reconstructions from PCA embeddings, where lower values indicate better generalization. **Grassmannian distance** (Lim et al., 2021) is the distance between two PCA subspaces for each mode in the PCA subspace. Thus, we introduce a new evaluation method that incorporates the PCA subspace derived from the SSM Grassmannian distance, where lower values indicate better performance. We report generalization and Grassmannian metrics for both strategy 1 and strategy 2.

### 3. Results and Discussion

**Performance of Semi-Supervised methods.** We report the Dice scores on test data in Table 1 when using 20% and 40% of labeled samples for training semi-supervised methods. Two noteworthy observations emerge from these results: (1) Not all semi-supervised methods show improved performance with an increasing amount of annotation data. In fact, for DeSCO and MT, we observe a very small decrease in performance as the amount of annotated data increases; (2) Nearly all models achieve a Dice score greater than 0.85 for the Left Atrium and 0.94 for the Femur. MCF emerges as the best-performing model, closely followed by BCP, while SASSnet and MT are the worst-performing models in terms of Dice score. Other segmentation performance metrics ASD, HD95 and Jaccard score are reported in appendix tables 2, 3 and 4, respectively. A similar trend is observed with these metrics. CAML and BCP consistently show lower surface distance metrics at both

Dataset	% Data	DeSCO	SASS	DTC	MCF	CAML	MT	UA-MT	BCP
<b>Left Atrium</b>	20 (8 labeled)	0.861	0.855	0.861	0.868	0.888	0.869	0.872	<b>0.896</b>
	40 (16 labeled)	0.840	0.885	0.881	<b>0.902</b>	0.892	0.859	0.873	0.901
<b>Femur</b>	20 (10 labeled)	0.954	0.949	<b>0.961</b>	0.958	0.959	0.930	0.943	<b>0.961</b>
	40 (20 labeled)	0.946	0.958	0.960	<b>0.974</b>	0.964	0.923	0.946	0.964

Table 1: **Semi-Supervised Segmentation Results.** Dice Score is reported on test data.

20% and 40% of the data, while MCF achieves the lowest surface distances when training semi-supervised methods with 40% of the data.

**Quantitative results for strategy 1.** Figure 2 presents the generalization and Grassmannian distance across different datasets when training semi-supervised methods with 20% and 40% of annotations. From the FEMUR results, we observe that test SSMs constructed

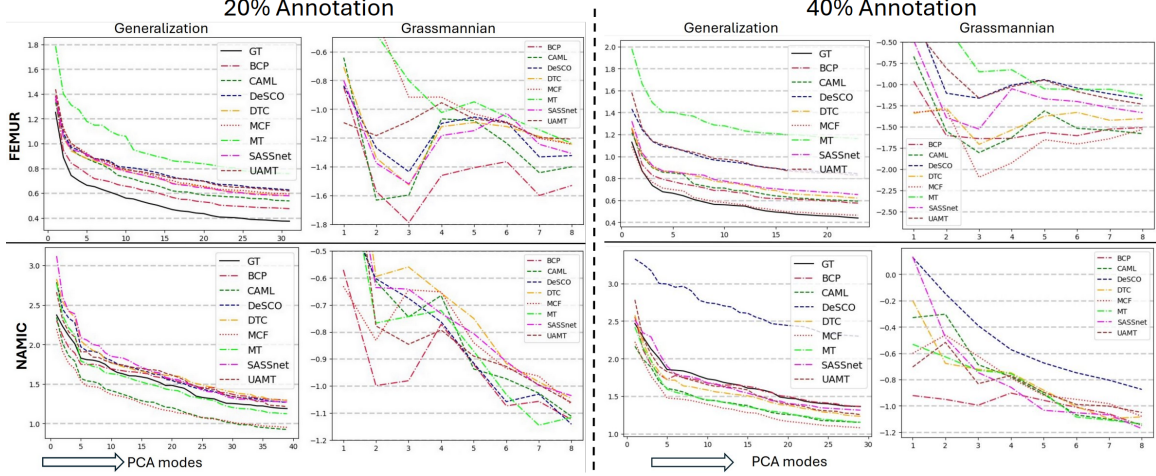


Figure 2: **Quantitative Results for strategy 1.** Generalization and log of Grassmannian distance reported for both FEMUR and NAMIC datasets when using 20% and 40% of annotations for training different semi-supervised methods.

using ground truth annotations consistently achieve lower generalization errors across all PCA modes compared to those derived from semi-supervised predictions, regardless of annotation usage (20% or 40%). Among the semi-supervised methods, BCP follows the GT model most closely in generalization performance, while CAML ranks third. In terms of Grassmannian distance, for models trained with 20% annotated data, BCP exhibits the lowest average distance per PCA mode, indicating that the PCA subspace of SSMs built from BCP-predicted test segmentations aligns most closely with the GT-based SSM. CAML follows as the next best-performing method. However, with 40% annotated data, MCF surpasses CAML in generalization performance, ranking second after GT, while BCP drops to third. Despite this shift, BCP maintains the lowest Grassmannian distance, with CAML and MCF closely following. Additionally, Grassmannian distances are lower in magnitude when using 40% of the data, suggesting that increasing annotation availability during semi-supervised training improves the underlying predicted SSM PCA subspace.

The NAMIC results reveal a different trend. When using 20% of the training data, CAML, MCF, and MT achieve better generalization scores than the Ground Truth (GT) SSM. This trend persists for nearly all weakly supervised methods, except DeSCO, when 40% of the data is used. Despite these improvements in generalization, the Grassmannian distance remains similar in magnitude to that observed with the FEMUR data, indicating that while generalization performance is higher for NAMIC, the PCA subspaces of the test SSMs and the GT-based SSM remain significantly different. Moreover, since the GT model’s generalization scores for NAMIC are comparable to all semi-supervised methods, this sug-

gests that test set SSMs constructed from either manual annotations or semi-supervised predictions are nearly indistinguishable for NAMIC dataset.

Lower generalization in semi-supervised methods does not imply that SSMs constructed with manual segmentation are inadequate; rather, they exhibit higher generalization errors due to distribution shifts between the training and test set segmentations done by radiologists. This result indicates that semi-supervised surface prediction is more consistent segmentation predictions across training and test sets, which is expected since many of these methods rely on entropy minimization or consistency-based approaches.

**Qualitative results for strategy 1.** Appendix Figure 5 illustrates the first mode of variation for the FEMUR and NAMIC datasets using 20% annotated data in semi-supervised models, while Figure 4 (Appendix B) presents the second mode of variation for both datasets. The results demonstrate that nearly all methods generate smooth and interpretable statistical shape models (SSMs), effectively capturing both the first and second modes. However, in some cases, the direction of variation is reversed in the test SSMs produced by semi-supervised models. Specifically, BCP, MT, and UAMT exhibit this reversal for both NAMIC and FEMUR in modes 1 and 2, while SASSnet also shows a reversed mode of variation for NAMIC in mode 1. Despite these reversals, all models successfully generate meaningful and accurate representations of shape variation.

**Quantitative Results for strategy 2.** Figure 3 (Appendix B) and Figure 8 (Appendix B) presents compactness, specificity, generalization and grassmannian distance for different datasets for models trained with 20% and 40% of annotations, respectively. For FEMUR, the ground truth SSM achieves the highest AUC for compactness, indicating that it is the most compact model, followed closely by CAML and BCP for both 20% and 40% annotated models. Generalization scores show a similar trend, with the GT SSM consistently performing best, followed by BCP and DTC as the second and third best models for 20% annotation, while MCF and DTC rank second and third for 40% annotation. In terms of specificity, DTC closely matches the GT SSM, with DeSCO ranking third for 20% models. For 40% models, SASSnet and BCP produce specificity scores that are also very similar to the GT SSM. The Grassmannian distance remains comparable to that observed in FEMUR results from strategy 1, indicating that the PCA subspace of test SSMs—whether initialized with the GT train SSM or the predicted train SSM—remains similarly distant.

For NAMIC, results align with strategy 1, where the GT model does not achieve the best generalization performance. Instead, DeSCO, MCF, and DTC emerge as the top-performing models in generalization. The GT model is also not the most compact; BCP performs best for 20% annotated models, while DTC ranks highest for 40% models. A similar pattern is observed for specificity scores. Unlike FEMUR, where increasing annotated data has little impact—as reflected by the unchanged Grassmannian distance—NAMIC shows a slight improvement in Grassmannian distance when moving from 20% to 40% annotation, suggesting that additional annotations provide a small but positive effect on SSM subspace alignment.

**Qualitative Results for strategy 2.** Figure 6 (Appendix B) illustrates the first mode of variation for the FEMUR and NAMIC datasets when using 20% annotated data for semi-supervised models, while Figure 7 (Appendix B) presents the second mode of variation for both datasets. From these figures, we observe that SSMs generated for the FEMUR dataset by BCP, CAML, DeSCO, and DTC exhibit smooth shapes, closely resembling the ground truth SSM, while other methods result in poor-quality SSM. Additionally, CAML,

DeSCO, and DTC effectively capture the first mode of variation, though are noticeable differences in BCP’s results. A similar trend is observed for NAMIC, where the same semi-supervised methods also produce smooth SSMs. However, none of the SSM models successfully capture the left atrium ventricles(all SSMs are blob like structures), leading to significantly noticeable discrepancies in both mode 1 and mode 2 compared to the GT SSM.

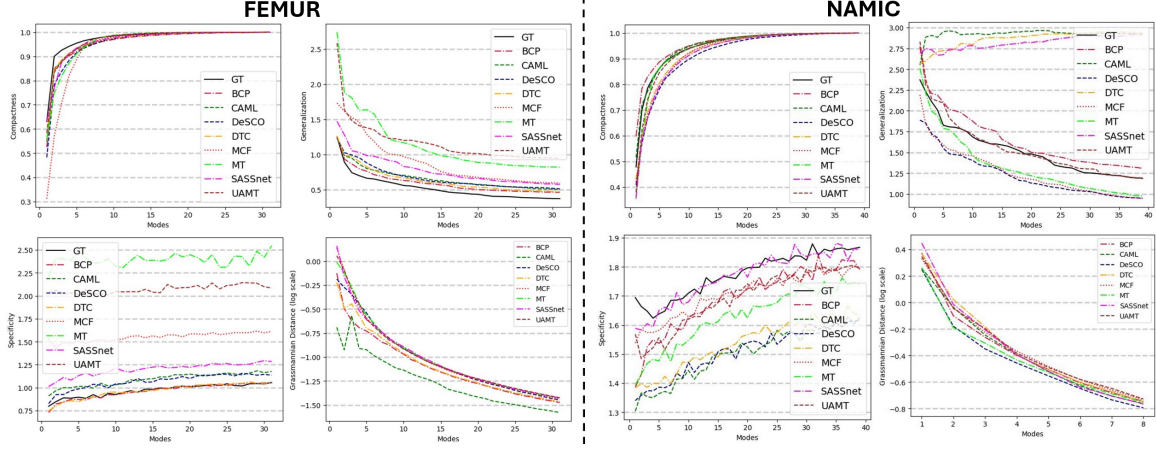


Figure 3: **Results when using 20% of Annotation for strategy 2.** Compactness, Specificity, Generalization and log of Grassmannian distance were reported for both both FEMUR and NAMIC datasets when using 20% of annotations for training different semi-supervised methods.

#### 4. Conclusion and Future Work

In this study, we address a critical bottleneck hindering the widespread adoption of statistical shape modeling (SSM) for diagnostic decision-making: the manual annotation burden. We investigate semi-supervised models as potential alternatives to manual segmentation and evaluate several such models on two datasets. Our qualitative and quantitative analyses reveal that when semi-supervised models are used exclusively for test-set prediction and SSM generation—while training SSMs rely on manual segmentations, strategy 1—the resulting test SSMs successfully capture the correct modes of variation, closely resembling the ground truth. However, this consistency does not hold when manual annotations are unavailable for SSM training (strategy 2). Notably, some semi-supervised methods, such as BCP, CAML, DeSCO, and DTC, prove to be viable alternatives to manual segmentation for the FEMUR dataset in strategy 2, producing smooth SSMs while accurately preserving the expected modes of variation. However, results from the NAMIC dataset are less promising. In particular, none of the semi-supervised methods successfully captured the ventricles in the left atrium, leading to substantial discrepancies between the generated SSMs and the ground truth SSMs. This limitation highlights a key challenge for future semi-supervised research: improving semi-supervised models to better predict small anatomical structures that are often overlooked by current approaches such as the left ventricle for NAMIC dataset. Moving forward, we plan to expand our comparison by incorporating a broader range of weakly supervised segmentation approaches, including self-supervised and unsupervised methods,

transfer learning strategies, and foundational models such as SAM ([Kirillov et al., 2023](#)) and Med-SAM ([Wang et al., 2023a](#)).



## References

- Jadie Adams and Shireen Elhabian. From images to probabilistic anatomical shapes: A deep variational bottleneck approach. *arXiv preprint arXiv:2205.06862*, 2022.
- Jadie Adams, Riddhish Bhalodia, and Shireen Elhabian. Uncertain-deepssm: From images to probabilistic shape models. In *Shape in Medical Imaging: International Workshop, ShapeMI 2020, Held in Conjunction with MICCAI 2020, Lima, Peru, October 4, 2020, Proceedings*, pages 57–72. Springer, 2020.
- Jadie Adams, Krithika Iyer, and Shireen Elhabian. Weakly supervised bayesian shape modeling from unsegmented medical images. *arXiv preprint arXiv:2405.09697*, 2024.
- Yunhao Bai, Duowen Chen, Qingli Li, Wei Shen, and Yan Wang. Bidirectional copy-paste for semi-supervised medical image segmentation. In *Proceedings of the IEEE/CVF Conference on Computer Vision and Pattern Recognition*, pages 11514–11524, 2023.
- Riddhish Bhalodia, Shireen Y Elhabian, Ladislav Kavan, and Ross T Whitaker. Deepssm: a deep learning framework for statistical shape modeling from raw images. In *Shape in Medical Imaging: International Workshop, ShapeMI 2018, Held in Conjunction with MICCAI 2018, Granada, Spain, September 20, 2018, Proceedings*, pages 244–257. Springer, 2018.
- Riddhish Bhalodia, Shireen Elhabian, Jadie Adams, Wenzheng Tao, Ladislav Kavan, and Ross Whitaker. Deepssm: A blueprint for image-to-shape deep learning models. *Medical Image Analysis*, 91:103034, 2024.
- Heng Cai, Shumeng Li, Lei Qi, Qian Yu, Yinghuan Shi, and Yang Gao. Orthogonal annotation benefits barely-supervised medical image segmentation. In *Proceedings of the IEEE/CVF Conference on Computer Vision and Pattern Recognition*, pages 3302–3311, 2023.
- Joshua Cates, Shireen Elhabian, and Ross Whitaker. Shapeworks: particle-based shape correspondence and visualization software. In *Statistical shape and deformation analysis*, pages 257–298. Elsevier, 2017.
- Shengbo Gao, Ziji Zhang, Jiechao Ma, Zihao Li, and Shu Zhang. Correlation-aware mutual learning for semi-supervised medical image segmentation. In *International Conference on Medical Image Computing and Computer-Assisted Intervention*, pages 98–108. Springer, 2023.
- Anupama Goparaju, Krithika Iyer, Alexandre Bone, Nan Hu, Heath B Henninger, Andrew E Anderson, Stanley Durrleman, Matthijs Jaxsens, Alan Morris, Ibolya Csecs, et al. Benchmarking off-the-shelf statistical shape modeling tools in clinical applications. *Medical Image Analysis*, 76:102271, 2022.
- Krithika Iyer and Shireen Y Elhabian. Mesh2ssm: From surface meshes to statistical shape models of anatomy. In *International Conference on Medical Image Computing and Computer-Assisted Intervention*, pages 615–625. Springer, 2023.

- Krithika Iyer, Jadie Adams, and Shireen Y Elhabian. Scorp: Statistics-informed dense correspondence prediction directly from unsegmented medical images. *arXiv preprint arXiv:2404.17967*, 2024.
- Mokshagna Sai Teja Karanam, Tushar Kataria, Krithika Iyer, and Shireen Y Elhabian. Adassm: Adversarial data augmentation in statistical shape models from images. In *International Workshop on Shape in Medical Imaging*, pages 90–104. Springer, 2023.
- Tushar Kataria, Beatrice Knudsen, and Shireen Elhabian. To pretrain or not to pretrain? a case study of domain-specific pretraining for semantic segmentation in histopathology. In *Workshop on Medical Image Learning with Limited and Noisy Data*, pages 246–256. Springer, 2023.
- Tushar Kataria, Beatrice S Knudsen, and Shireen Y Elhabian. Unsupervised domain adaptation for semantic segmentation under target data scarcity. In *2024 IEEE International Symposium on Biomedical Imaging (ISBI)*, pages 1–5. IEEE, 2024.
- Alexander Kirillov, Eric Mintun, Nikhila Ravi, Hanzi Mao, Chloe Rolland, Laura Gustafson, Tete Xiao, Spencer Whitehead, Alexander C Berg, Wan-Yen Lo, et al. Segment anything. In *Proceedings of the IEEE/CVF International Conference on Computer Vision*, pages 4015–4026, 2023.
- Shuailin Li, Chuyu Zhang, and Xuming He. Shape-aware semi-supervised 3d semantic segmentation for medical images. In *Medical Image Computing and Computer Assisted Intervention—MICCAI 2020: 23rd International Conference, Lima, Peru, October 4–8, 2020, Proceedings, Part I 23*, pages 552–561. Springer, 2020.
- Shumeng Li, Heng Cai, Lei Qi, Qian Yu, Yinghuan Shi, and Yang Gao. Pln: Parasitic-like network for barely supervised medical image segmentation. *IEEE Transactions on Medical Imaging*, 42(3):582–593, 2022.
- Lek-Heng Lim, Ken Sze-Wai Wong, and Ke Ye. The grassmannian of affine subspaces. *Found. Comput. Math.*, 21:537–574, Mar 2021. doi: 10.1007/s10208-020-09459-8.
- Xiangde Luo, Jieneng Chen, Tao Song, and Guotai Wang. Semi-supervised medical image segmentation through dual-task consistency. In *Proceedings of the AAAI conference on artificial intelligence*, volume 35, pages 8801–8809, 2021.
- Fausto Milletari, Alex Rothberg, Jimmy Jia, and Michal Sofka. Integrating statistical prior knowledge into convolutional neural networks. In *International Conference on Medical Image Computing and Computer-Assisted Intervention*, pages 161–168. Springer, 2017.
- Rachael Nihalaani, Tushar Kataria, Jadie Adams, and Shireen Y Elhabian. Estimation and analysis of slice propagation uncertainty in 3d anatomy segmentation. In *International Conference on Medical Image Computing and Computer-Assisted Intervention*, pages 273–285. Springer, 2024.
- Ashwin Raju, Shun Miao, Dakai Jin, Le Lu, Junzhou Huang, and Adam P Harrison. Deep implicit statistical shape models for 3d medical image delineation. In *Proceedings of the AAAI Conference on Artificial Intelligence*, volume 36, pages 2135–2143, 2022.

- Wenzheng Tao, Riddhish Bhalodia, and Shireen Elhabian. Learning population-level shape statistics and anatomy segmentation from images: A joint deep learning model. *arXiv preprint arXiv:2201.03481*, 2022.
- Antti Tarvainen and Harri Valpola. Mean teachers are better role models: Weight-averaged consistency targets improve semi-supervised deep learning results. *Advances in neural information processing systems*, 30, 2017.
- Janmesh Ukey and Shireen Elhabian. Localization-aware deep learning framework for statistical shape modeling directly from images. In *Medical Imaging with Deep Learning*, 2023.
- Janmesh Ukey, Tushar Kataria, and Shireen Y Elhabian. MASSM: An end-to-end deep learning framework for multi-anatomy statistical shape modeling directly from images. 2024. doi: 10.48550/arXiv.2403.11008. Retrieved from URL.
- Tuan-Hung Vu, Himalaya Jain, Maxime Bucher, Matthieu Cord, and Patrick Pérez. Advent: Adversarial entropy minimization for domain adaptation in semantic segmentation. In *Proceedings of the IEEE/CVF conference on computer vision and pattern recognition*, pages 2517–2526, 2019.
- Haoyu Wang, Sizheng Guo, Jin Ye, Zhongying Deng, Junlong Cheng, Tianbin Li, Jianpin Chen, Yanzhou Su, Ziyang Huang, Yiqing Shen, Bin Fu, Shaoting Zhang, Junjun He, and Yu Qiao. Sam-med3d, 2023a.
- Yongchao Wang, Bin Xiao, Xiuli Bi, Weisheng Li, and Xinbo Gao. Mcf: Mutual correction framework for semi-supervised medical image segmentation. In *Proceedings of the IEEE/CVF conference on computer vision and pattern recognition*, pages 15651–15660, 2023b.
- Lijun Wu, Juntao Li, Yue Wang, Qi Meng, Tao Qin, Wei Chen, Min Zhang, Tie-Yan Liu, et al. R-drop: Regularized dropout for neural networks. *Advances in Neural Information Processing Systems*, 34:10890–10905, 2021.
- Jin Xie, Guoxian Dai, Fan Zhu, Edward K Wong, and Yi Fang. Deepshape: Deep-learned shape descriptor for 3d shape retrieval. *IEEE transactions on pattern analysis and machine intelligence*, 39(7):1335–1345, 2016.
- Hong Xu and Shireen Y Elhabian. Image2ssm: Reimagining statistical shape models from images with radial basis functions. *arXiv preprint arXiv:2305.11946*, 2023.
- Pak-Hei Yeung, Ana IL Namburete, and Weidi Xie. Sli2vol: Annotate a 3d volume from a single slice with self-supervised learning. In *Medical Image Computing and Computer Assisted Intervention–MICCAI 2021: 24th International Conference, Strasbourg, France, September 27–October 1, 2021, Proceedings, Part II 24*, pages 69–79. Springer, 2021.
- Lequan Yu, Shujun Wang, Xiaomeng Li, Chi-Wing Fu, and Pheng-Ann Heng. Uncertainty-aware self-ensembling model for semi-supervised 3d left atrium segmentation. In *Medical*

*Image Computing and Computer Assisted Intervention–MICCAI 2019: 22nd International Conference, Shenzhen, China, October 13–17, 2019, Proceedings, Part II 22*, pages 605–613. Springer, 2019.

## Appendix A. Additional Dataset and Implementation Details

We evaluated two levels of labeled data availability for training the semi-supervised models. Specifically, for the in-house dataset(FEMUR), we used 20% labeled samples (8 labeled, 32 unlabeled) and 40% labeled samples (16 labeled, 24 unlabeled). Similarly, for the public Left Atrium dataset(NAMIC), we split the data into 50 training and 9 testing samples, utilizing 20% labeled samples (10 labeled, 40 unlabeled) and 40% labeled samples (20 labeled, 30 unlabeled) for training.

**Implementation Details.** Original implementation with default parameters were used for all Semi-Supervised methods. All semi-supervised models were trained on NVIDIA GPU 1080ti with 12GB, except CAML which was trained on A100 with 40GB RAM because the model did not fit in 12GB RAM. ShapeWorks (Cates et al., 2017) was chosen as the tool to create all shape models for analysis because of its high efficacy (Goparaju et al., 2022).

## Appendix B. Additional Results

Dataset	% Data	DeSCO	SASS	DTC	MCF	CAML	MT	UA-MT	BCP
<b>Left</b>	20 (8 labeled)	1.81	2.16	1.83	2.01	<b>1.31</b>	2.02	2.93	1.53
<b>Atrium</b>	40 (16 labeled)	4.51	1.41	1.49	1.34	<b>1.30</b>	1.59	1.68	1.34
<b>Femur</b>	20 (10 labeled)	0.92	1.57	0.76	1.56	0.84	3.99	2.72	<b>0.68</b>
	40 (20 labeled)	1.40	0.76	0.67	<b>0.53</b>	0.689	2.32	1.93	0.65

Table 2: **Average Surface Distance Metric for Segmentation.** Lower is better.

Dataset	% Data	DeSCO	SASS	DTC	MCF	CAML	MT	UA-MT	BCP
<b>Left</b>	20 (8 labeled)	7.16	8.92	7.80	7.77	6.17	7.84	10.40	<b>5.86</b>
<b>Atrium</b>	40 (16 labeled)	15.53	5.60	6.19	<b>4.62</b>	6.12	7.30	6.65	4.71
<b>Femur</b>	20 (10 labeled)	2.60	5.14	2.38	3.98	2.85	15.52	9.67	<b>2.04</b>
	40 (20 labeled)	5.18	2.47	2.30	<b>1.48</b>	2.45	6.7	7.28	2.0

Table 3: **Hausdorff Distance Metric for Segmentation.** Lower is better

Dataset	% Data	DeSCO	SASS	DTC	MCF	CAML	MT	UA-MT	BCP
<b>Left</b>	20 (8 labeled)	0.757	0.747	0.757	0.767	0.800	0.769	0.773	<b>0.812</b>
<b>Atrium</b>	40 (16 labeled)	0.727	0.795	0.788	<b>0.822</b>	0.807	0.754	0.776	0.821
<b>Femur</b>	20 (10 labeled)	0.912	0.904	<b>0.925</b>	0.921	0.922	0.871	0.894	<b>0.926</b>
	40 (20 labeled)	0.899	0.919	0.924	<b>0.950</b>	0.931	0.862	0.898	0.930

Table 4: **Jaccard Score Metric for Segmentation.** Higher is better.

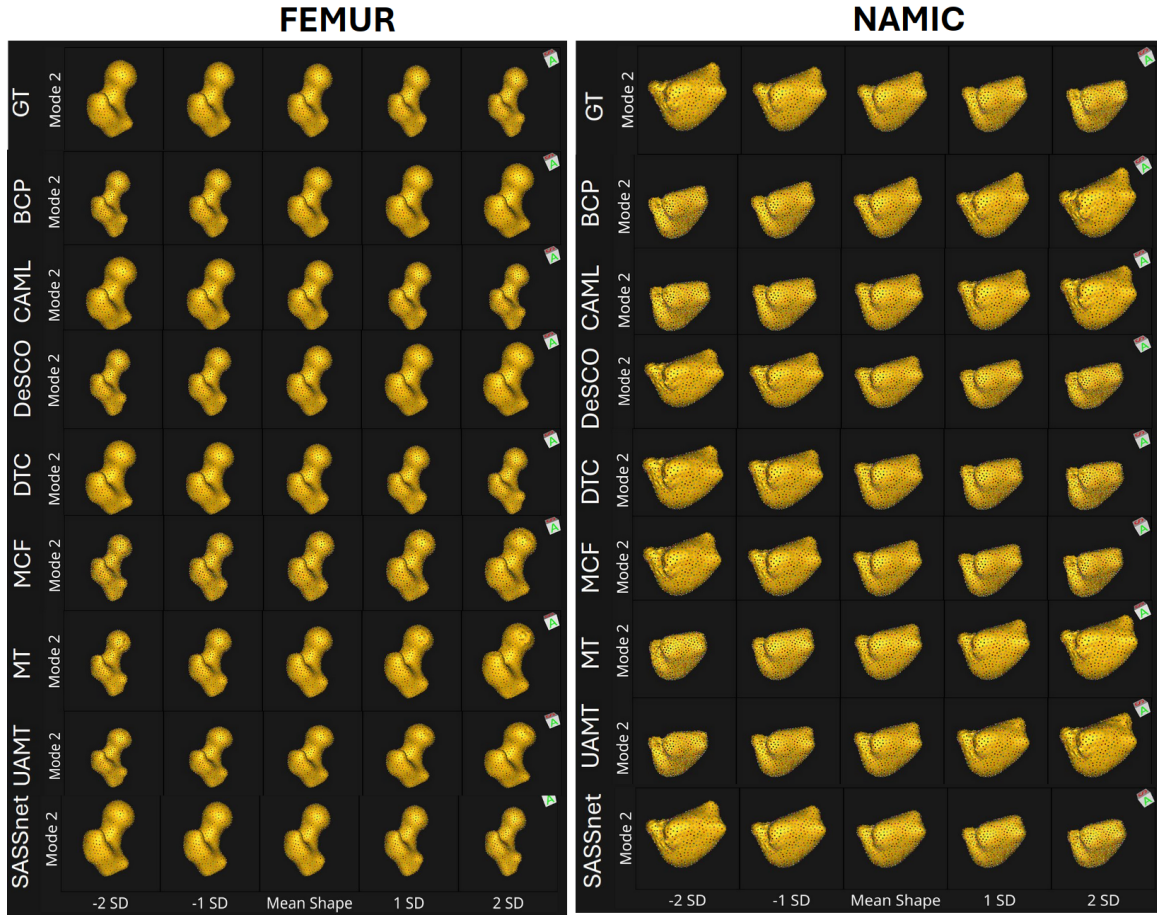


Figure 4: **Qualitative Results for FEMUR and NAMIC dataset showing Second mode of variation for Strategy 1.** Second Mode of Variation when SSM is created using segmentation predicted by semi-supervised models trained on 20% of the training data.

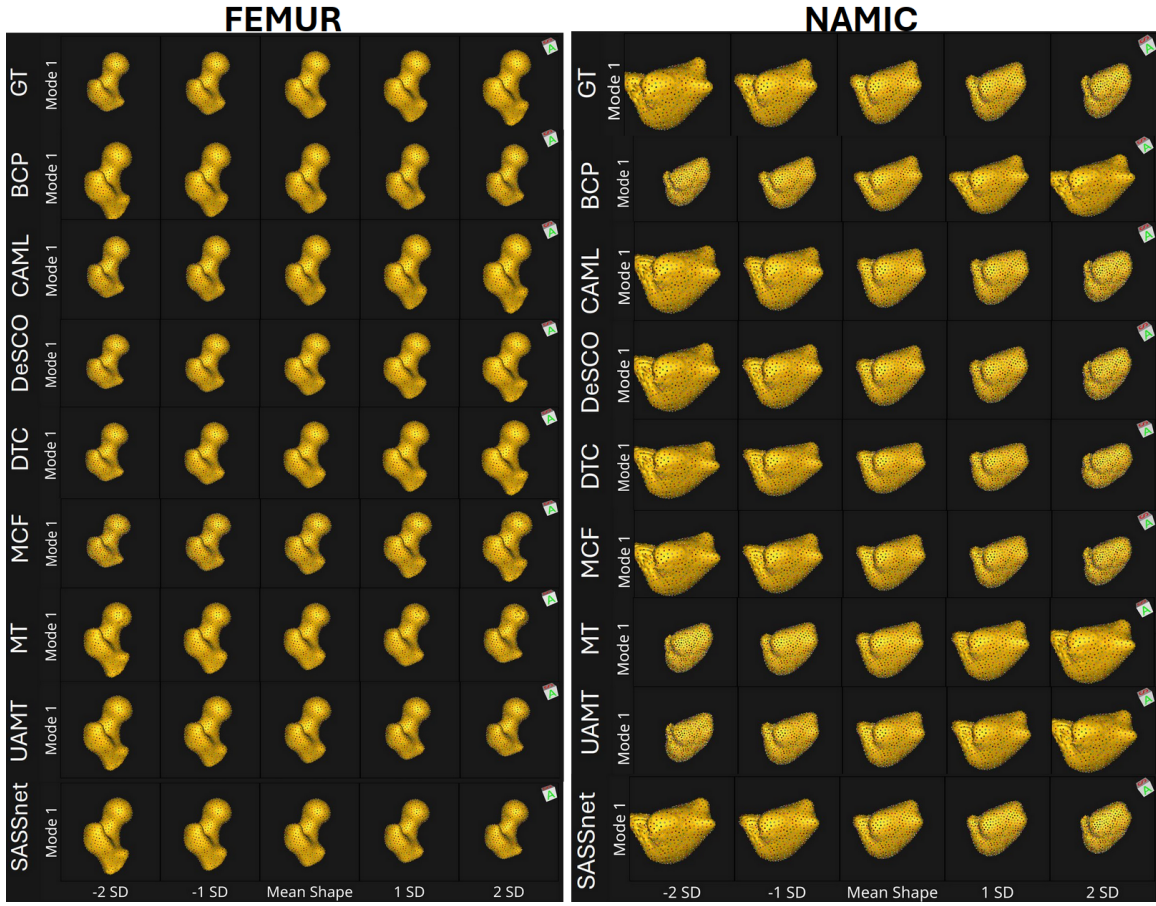


Figure 5: **First Mode Of variation Results for FEMUR and NAMIC using 20% of labelled data for strategy 1** . We show first mode of variations for both Femur and Left Atrium datasets showing mean shape( $\mu$ ), first ( $\pm\sigma$ ) and second order ( $\pm2\sigma$ ) variations from mean shape.



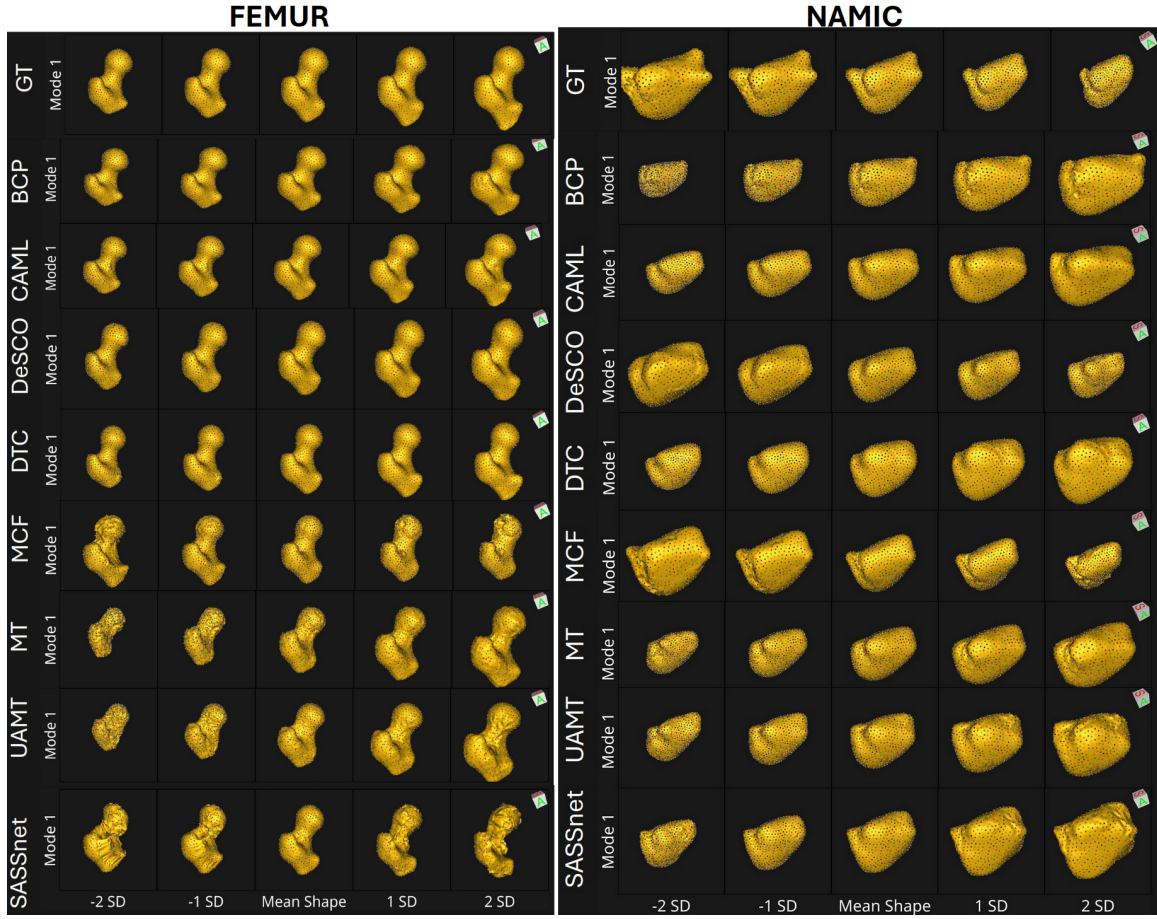


Figure 6: **First Mode Of variation Results for FEMUR and NAMIC using 20% of labelled data for strategy 2** . We show first mode of variations for both Femur and Left Atrium datasets showing mean shape( $\mu$ ), first ( $\pm\sigma$ ) and second order ( $\pm 2\sigma$ ) variations from mean shape.

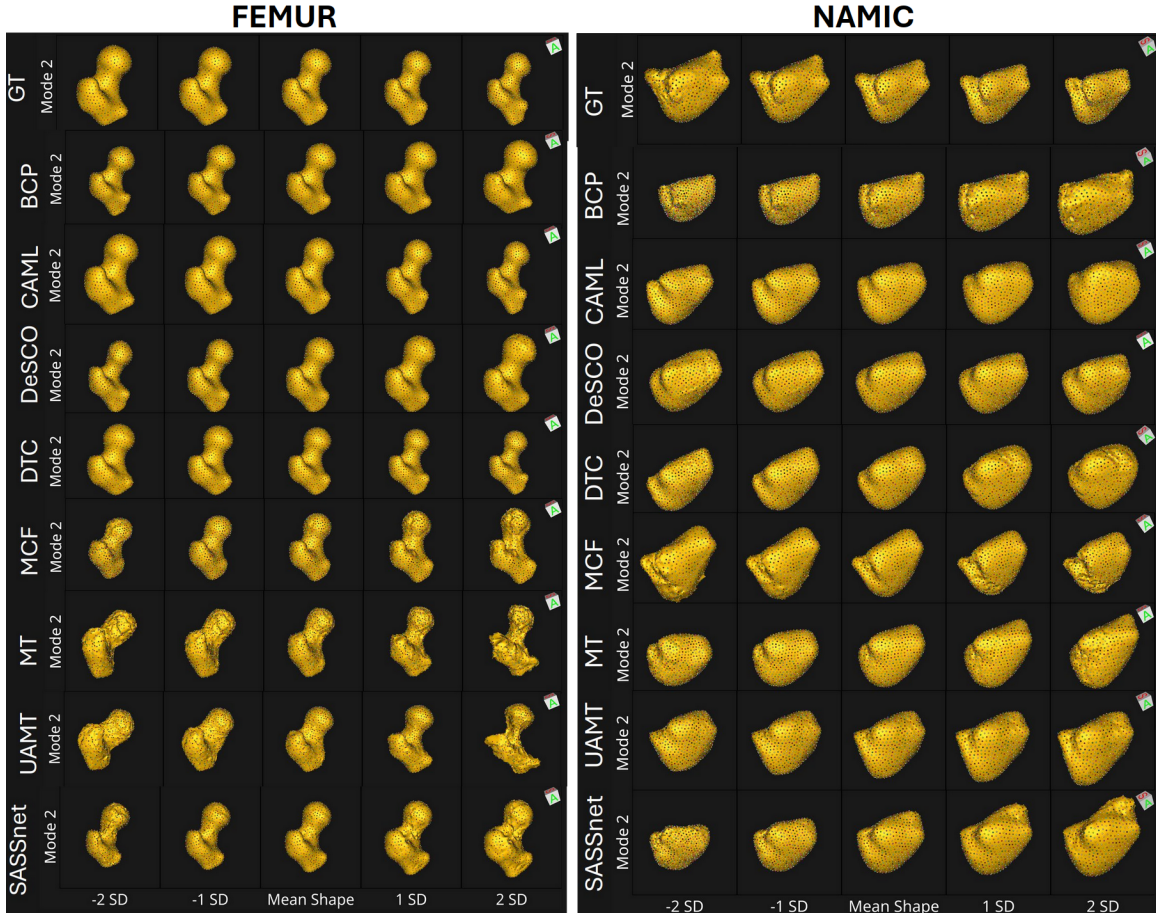


Figure 7: **Qualitative Results for FEMUR and NAMIC dataset showing Second mode of variation for Strategy 2.** Second Mode of Variation when SSM is created using segmentation predicted by semi-supervised models trained on 20% of the training data.

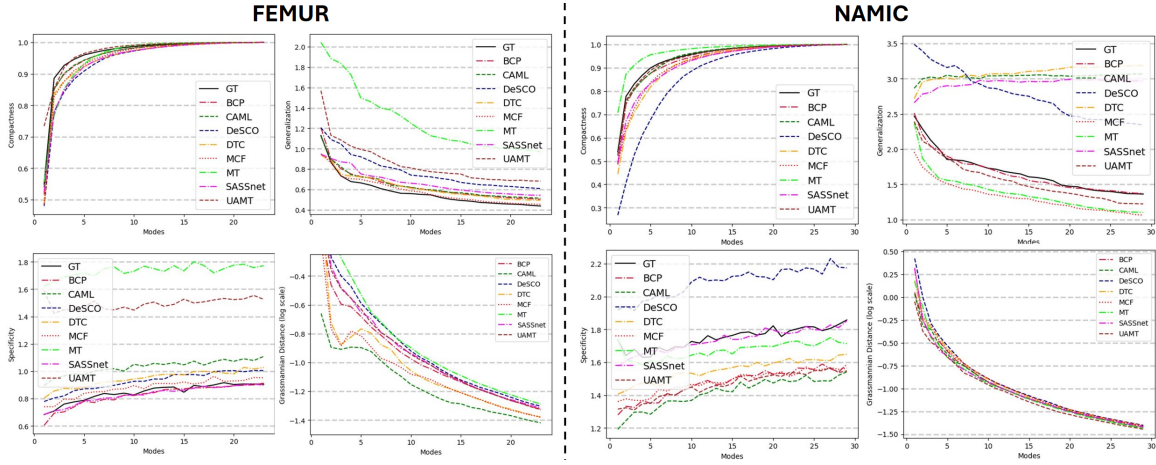


Figure 8: **Strategy 2 Results when using 40% of Annotation.** Compactness, Specificity, Generalization and Grassmannian distance reported for both both FEMUR and NAMIC datasets when using 40% of annotations for training different semi-supervised methods.

